Published in final edited form as:
Magn Reson Med. 2014 May ; 71(5): 1932–1943. doi:10.1002/mrm.24841.

Evaluation of Coils for Imaging Histological Slides: Signal-to-Noise Ratio and Filling Factor

Dung Minh Hoang[1,2], **Evelyn B. Voura**[1,3,4], **Chao Zhang**[1], **Latifa Fakri-Bouchet**[2], and **Youssef Zaim Wadghiri**[1,*]

[1]The Bernard & Irene Schwartz Center for Biomedical Imaging, Department of Radiology, New York University Langone Medical Center (NYULMC), New York, New York, USA

[2]Creatis-LRMN, UMR CNRS 5220, INSERM U 630, Université Lyon 1, Villeurbanne, France

[3]Department of Biology, Dominican College, Orangeburg, New York, USA

[4]Department of Neurosurgery, New York University Langone Medical Center (NYULMC), New York, New York, USA

Abstract

Purpose—To investigate the relative gain in sensitivity of five histology coils designed in-house to accommodate tissue sections of various sizes and compare with commercial mouse head coils.

Methods—The coil set was tailored to house tissue sections ranging from 5 to 1000 μm encased in either glass slides or coverslips.

Results—Our simulations and experimental measurements demonstrated that although the sensitivity of this flat structure consistently underperforms relative to a birdcage head coil based on the gain expected from their respective filling factor ratios, our results demonstrate that it can still provide a remarkable gain in sensitivity. Our study also describes preparation protocols for freshly excised sections, as well as pre-mounted tissue slides of both mouse and human specimens. Examples of the exceptional level of tissue detail and the near-perfect magnetic resonance imaging to light microscopic image coregistration are provided.

Conclusion—The increase in filling factor achieved by the histology radiofrequency (RF) probe overcomes the losses associated with electric leaks inherent to this structure, leading to a 6.7-fold improvement in performance for the smallest coil implemented. Alternatively, the largest histology coil design exhibited equal sensitivity to the mouse head coil while nearly doubling the RF planar area coverage.

Keywords

MR microscopy; RF coil design; MR histology; filling factor; coregistration

*Correspondence to: Youssef Zaim Wadghiri, Ph.D., The Bernard and Irene Schwartz, Center for Biomedical Imaging, Department of Radiology, New York University Langone Medical Center (NYULMC), New York, NY, USA. wadghiri@med.nyu.edu.

Additional Supporting Information may be found in the online version of this article.

In biomedical research, the use of animal models of human disease offers the opportunity to test and optimize magnetic resonance imaging (MRI) pulse sequences, and to compare image features with corresponding histopathology, the current gold standard for disease assessment. Despite these great advantages, the coregistration steps between MRI and histological sections obtained through light microscopy have presented important practical challenges (1–5). The main difficulties encountered during the validation steps stem from both the slice section misalignments and the significant difference in slice thicknesses between sub-millimetric in vivo MRI (ranging from 100 μm to 1 mm thickness) and histology sections (thicknesses commonly ranging from 5 to 100 μm). These limitations have been partially addressed by acquiring three-dimensional (3D) ex vivo images of excised and perfused organs of interest. The scanning is usually assessed over long imaging times using a dedicated coil closely fitting the sample to improve the sensitivity (6–20). The accumulation of repeated scans results in motion-free and highly resolved 3D MRI datasets enabling a precise virtual realignment of the image slice of interest to closely match the physical histology section (21–26).

However, important discrepancies remain between these two analyses (22). These notable differences can be attributed to sample changes associated with postmortem tissue processing due to fixation and dehydration resulting in tissue deformation, as well as artifacts caused by sectioning and the chemicals used during the staining process (27–33). These discrepancies have been addressed using time-consuming postprocessing techniques when establishing 3D atlases (21–24). But this approach may be more difficult to systematically implement for every existing transgenic mouse line or murine disease model due to limited resources or lack of image postprocessing expertise.

Alternatively, histological slides can conceivably be scanned directly by both MRI and light microscopy (34–36). Coregistration would then be easily achievable provided that MRI sensitivity and the experimental conditions allow direct imaging with adequate spatial resolution of histological sections ranging from 5 to 100 μm. Along these lines, efforts have been devoted to the design of dedicated radiofrequency (RF) coil geometries that closely matches the shape of the tissue of interest. Nabuurs and coworkers (36) proposed the use of an inductively coupled loop combined with a commercial linear birdcage mouse head coil capable of housing the slide setup. The insertion of the coupled loop was aimed at driving the effective RF coverage toward the tissue of interest thereby reciprocally increasing the resulting sensitivity. This solution led to a less than fourfold gain in sensitivity under the best geometrical inductive coupling conditions compared with results obtained using the linear birdcage mouse head coil alone. Alternatively, Meadowcroft et al. (35) proposed a unique RF coil design based on a flat U-shaped structure that closely matches the planar nature of a histological tissue sample providing the most optimal filling factor. The authors demonstrated excellent RF homogeneity throughout the region of interest (24 × 24 mm) within the coil cavity designed to house a sample encased on dual glass coverslips. The length (L) of the coil was doubled (L = 48 mm) by inserting an equal-sized Teflon spacer between the two flat copper strips next to the U-shaped cavity leading to the driving port. The presence of this spacer both provided some distributed capacitance and allowed for the

current to be spread evenly throughout the strip before reaching the sample cavity from the connections to the tuning capacitor.

Although the sensitivity of this new probe design was not compared with other commonly available RF coil structures, the authors demonstrated their ability to acquire highly detailed MRI from 60 μm sections of freshly mounted tissue sandwiched between two coverslips. This setup enabled the accurate correlation between MRI and light microscopy by direct imaging of postmortem tissue samples from either human Alzheimer's Disease (AD) subjects or mice of a strain exhibiting some characteristics of AD (34).

Here, we build on the work of Meadowcroft et al. to accommodate both wider and thicker tissue slides by devising an in-house set of five histology MRI probes. All newly designed RF histology resonators were systemically characterized by mapping their RF homogeneity and examining how each performed against commercially available surface and whole mouse head coils. In addition, we examined the effect of the spacer on the resulting coil sensitivity by replacing the Teflon with either air or glass as alternative insulators.

We intended to image both freshly mounted tissue and premounted specimens originating from either paraffin embedding or cryosections having thicknesses ranging from 5 to 1000 μm. To this effect, our study investigated the best conditions for sample preparation for either case in order to minimize MRI artifacts. We demonstrated that our new five-coil set can accommodate off-the-shelf standardized histology preparations ranging from dual coverslips to glass slides. MRI examples of tissue derived from whole mouse organs and human specimens illustrate both the performance of each coil, as well as the near perfect coregistration with histology.

METHODS

RF Coils

Histology Coil Design—All coils designed for this study were made from a copper adhesive tape carefully cut and fixed on Plexiglas supports. The specific height of the sample insertion gap was achieved by designing in-house low permittivity spacers using layers of Teflon tape (Fig. 1). Similarly, a glass-based spacer was also fabricated in-house using layers of stacked #1 glass coverslips to achieve the overall desired glass height.

Each RF resonator was pretuned with a fixed capacitor to an upper resonance before being readjusted to the Larmor frequency via a turning/matching (T/M) network (37) (Fig. 1) integrated within a dedicated holder. Ease of histology coil interchange was achieved via a 3-cm-long double-shielded coaxial cable and BNC connector to minimize cable losses while enabling an adequate distance from the T/M box to prevent static magnetic field perturbation in the sample.

RF Coil Characterization

Filling Factor (η)—The filling factor, a measure of the geometrical correspondence between the RF coil and the sample being studied, is defined as the ratio of the magnetic field energy stored inside the sample volume versus the total magnetic energy stored by the

RF coil (38). Traditionally, this is expressed as a ratio of the volume of the sample to the volume of the coil assuming a homogeneous coil RF field (39). In practical terms, this translates into fitting the coil closely to the sample of interest to achieve a high filling factor. However, in our study, the needs and challenges associated with measuring the effective sample volumes were circumvented by evaluating the filling factor relative to a circularly polarized (CP) commercially available whole mouse head Litz coil (inner diameter (ID) = 28 mm, accessible ID = 26 mm, length (*L*) =29 mm; Doty Scientific, Columbia, SC). Using this as a reference throughout this study eased the practical calculation of the relative filling factor (η_R) as the ratio between the inner volumes of each histology coil and the mouse head coil irrespective of the sample size. With this approach, we assumed that the inner volume of each coil is similar to their effective RF B_1 volume. The Doty mouse head Litz coil, providing the largest RF volume was set as our baseline, leading to a normalized unitary filling factor (η_R). However, this evaluation was not feasible with the surface coil due to its open structure, shape, and the inhomogeneous nature of the RF field.

Quality Factor—The electrical quality factor (*Q*), a measure of the contribution of power losses, was systematically measured for each coil tuned at 301 MHz and matched to 50 Ω both unloaded (Q_U) and loaded (Q_L) using a 60 μm tissue section as the sample load. The *Q* was measured with a network analyzer (Hewlett Packard 4396A) based on the reflection mode method (40). However, two of the commercial Bruker coils considered in this study were equipped with dedicated RF connectors that did not permit an assessment of their characterization under the same conditions used on the other probes. Similar to η_R, the relative quality factor (Q_R) was also calculated as the ratio of Q_L in each histology coil to that of the mouse head probe. The Q_R was assessed using our comparative characterization to account for the effect of Q_L on the resulting performance of each probe.

RF Coil Sensitivity

For practical reasons, the RF sensitivity of a coil is commonly formulated into a factor S_{RF} depending on both the filling factor (η) and the quality factor (*Q*) (38,39). Using the same sample acquired under identical experimental conditions, this dependence can be simplified into the $\eta \times Q$ product assuming that the magnetic coupling of the coil is uniform over the sample as (38):

$$S_{\mathrm{RF}} \approx K\sqrt{\eta \times Q} \quad [1]$$

In this expression, the constant *K* assumes that the following parameters are unchanged according to our experimental setup: Larmor frequency ω_0, the magnetic permeability of free space, μ_0, as well as the temperature T_{eq}, and the volume V_S, of the sample. To account for the effect of quadrature detection in the commercial coils compared with the linear nature of the histology coils, the sensitivity of the volume coils and projections with η were also divided by 1.4.

The characterization of the sensitivity against the gain in filling factor for all the coils was assessed relative to the whole mouse head CP probe—considered as our point of reference—with 100% sensitivity and a relative filling factor of $\eta_R = 1$. This was translated

experimentally using a 1-mm-thick brain tissue section encased in two coverslips to provide the greatest signal-to-noise ratio (SNR) achievable for the following coils, each capable of housing this sample size: (1) the two histology coils designed to accommodate glass slides, (2) a Bruker whole mouse head CP birdcage coil (ID = 24.5 mm, L = 28 mm, Model No. 1P T20063V3, referred as "Bruker head coil"), and (3) a Bruker 2-channel phased array receive-only mouse head surface coil (Model No. 1P T11204V3 referred as Bruker surface coil). The latter is a rectangular shaped probe (27 mm along X-direction × 19 mm along Z-direction) curved around a cylinder (ID = 25 mm). A 60-μm-thick tissue section encased between two 12 × 24 mm coverslips was considered for the comparative performance of the three remaining histology coils.

Dielectric Constant (ε)—The dielectric constant (also termed as permittivity ε) of all the spacers used in this study was assessed using a Network Analyzer (Hewlett Packard 4396A) (for more details see Supporting Information).

Phantom and Sample Preparation

RF Homogeneity Evaluation—A set of thin-layer phantoms filled with water doped with 2.5 mM Gd-DTPA was generated to qualitatively assess the overall RF homogeneity of each coil.

Fresh Tissue Sectioning and Mounting—Unless stated otherwise, all tissue sections used in this study were obtained from organs extracted from C57 black wild-type mice using previously described protocols (41). Procedures were performed in accordance with the Institutional Animal Care and Use Committee at the New York University School of Medicine. Slice thicknesses of cryosections ranged from 30 to 60 μm. Prior to mounting on a coverslip or glass slide for imaging, tissue sections were immersed in degassed buffer solution for rehydration while minimizing microbubbles formation that can be detrimental to MRI quality. A second coverslip was used to sandwich and seal the tissue, thereby preventing dehydration during MR scanning. The overall resulting sample thickness was less than 400 μm for a 100 μm tissue section encased between two coverslips and less than 1250 μm for a glass slide/coverslip combination.

Premounted Tissue—Tissue sections that were already mounted within a coverslip/glass slide required removal of the protective coverslip using xylene. The resulting unprotected section remained mounted on the glass slide and was then immersed and rehydrated in degassed PBS for 1 h before protective re-encasing with a #1 coverslip using the identical steps to the fresh tissue mounting protocol.

MRI Data Acquisition

MRI System—All MRI scans were performed on a 7T micro-MRI system consisting of a 7-Telsa 200-mm horizontal bore magnet (Magnex Scientific Ltd., Yarnton, UK) equipped with an actively shielded gradient coil (BGA-9S; ID 90-mm, 770-mT/m gradient strength, 100-μs rise time) interfaced to a Bruker Biospec console.

MRI Pulse Sequences—For the rapid and qualitative evaluation of the RF homogeneity using the doped water phantoms, a 2D spoiled gradient recalled sequence with 100-μm resolution was used with the following parameters: TR/TE = 50/10 ms, FOV = 5.12 × 5.12 cm, matrix = 512 × 512, NA = 16, flip angle (FA) = 50° and imaging time of 6 min 49 s.

A 2D multigradient echo was used to acquire an echo train within the same TR and generate a T2*-weighted dataset through four echo-averages with the following parameters: TR = 100 ms, TE = 3.2 ms. Echo spacing was varied to maximize tissue contrast based on the properties of the sample examined. The bandwidth (BW) was set to 293 Hz/pixel. The FA was adjusted to maximize SNR by reaching the empirical Ernst angle (42) in each experiment to account for the sample preparation and tissue shelf life. When faced with duty cycle limitations for T2*-weighted imaging with the highest spatial resolution, a single echo 2D-FLASH was used instead to sequentially acquire the varying TEs empirically imposed by the tissue sample. For T1-weighted MRI, keeping all parameters constant (TR = 100 ms, BW: 293Hz/pixel), TE was set to the minimum and FA was empirically adjusted to maximize the tissue contrast while ensuring an overall SNR over the entire tissue of greater than 40 (SNR measurement described in the data analysis). This was achievable by acquiring a series of low spatial resolution images (200-μm in-plane) followed by a region-of-interest (ROI)-based analysis to accordingly adjust the number of averages for a 10-h imaging time for an overnight unattended scan.

Both matrix and FOV settings were varied depending on the dimensions of the samples leading to an in-plane resolution ranging from 30 to 100 μm.

Histology and Data Analysis

All the histological images were acquired at 5× magnification using a Leica microscope and were stitched together using Photoshop. All the acquired images were examined and analyzed using ImageJ free-ware. The homogeneity of the RF field for each coil was qualitatively assessed via a pixel-based color-coded map displaying the homogenous region within the 10% deviation from the mean signal intensity at the center of the coil and 5% relative increments.

RESULTS

The design of our histology coil was based on off-the-shelve materials requiring a simple construction as depicted in Figure 1. The assembly was made in-house using Plexiglas as a support, copper tape to conduct the current, and thermo-glue to keep the structure together as shown in Figure 1b, d. The size of the resulting planar coil structure was dictated by the size of the tissue sections examined, as well as by the width and thickness of the glass support available. For samples encased by two coverslips, a coil with an opening height of 450 μm housed sections as thick as 130 μm. The surface area covering the imaging of the tissue depended on the width (*W*) of the flat copper strip (Fig. 1a).

For this work, three widths (*W* = 12, 26, and 52 mm) were chosen to image a variety of tissue sections ranging from organ subsections from the mouse olfactory bulb to large samples such as whole mouse organ slices or human specimens. The 150-μm-thick glass

coverslips used in our study were either 12 or 24 mm wide resulting in the design of coils with the same corresponding inner length of the insert (IL = 12 and 24 mm) in order to accommodate the encased samples (Fig. 1c). The U-shaped slotted resonator outer length (OL) was extended by an adequate length of the Teflon-based capacitor to ensure the even spread of the surface current within the copper tape before reaching the edge of the opening. The choice of a capacitor of equal length to the IL of the insert was based on Meadowcroft et al.'s simulation (35). The adjustment of the resonance frequency was achieved by a homemade T/M circuit based on two variable capacitors (Voltronics Corps., Salisbury, MD) (Fig. 1f). Our setup was designed to ensure that all of our probes could easily interface with the same T/M circuit via a RG223 double-shielded coaxial cable using a BNC connector.

The combination of the various dimensions (*W*, IL, OL, and *H*) led to the design of five distinct histology coils comprised of three planar coil dimensions (*W* × IL, referred to as small: 12 × 12 mm; medium: 26 × 24 mm; and large: 52 × 24 mm, respectively) as depicted in Figure 2a. The systematic choice of OL = 2× IL demonstrated a homogeneous RF field coverage throughout the cavity housing the tissue sample for all the coils (Fig. 2b). Two opening heights (*H* = 450 and 1350 μm) were included in the coil set to enable the insertion of either encasing style (slide with coverslip or dual coverslip) covering tissue thicknesses ranging from 5 to 1000 μm (Fig. 2c, d).

Characterization and Sensitivity of the Histology Coils

In order to gauge the gain in performance of all the MRI probes designed for this study relative to a standard small animal coil setup such as a mouse head imaging setup, we systematically characterized the η_R, Q_U, Q_L, and Q_R for each RF resonator when possible and conducted a comparative evaluation of their relative sensitivity S_R as summarized in Figure 3. The S_R evaluation was made by calculating the effective SNR between each coil and the reference head coil described previously (see above) using the same sample and normalized to 100% sensitivity for filling factor of unity. A 6.7-fold gain in sensitivity was obtained with the smallest histology structure, which accommodated tissue sections ranging in thickness from 5 to 100 μm. This significant performance enhancement was achieved predominantly thanks to the gain in filling factor and a marginal improvement of the *Q* factor in comparison with larger histology structures.

A comparison of the S_R sensitivity for all the probes relative to their filling factor was also established as a plot in Figure 4. The continuous line shows the theoretical increase in sensitivity that would result from the reference head coil (filled circle, $\eta_R = 1$, $S_R = 100\%$) relative to the gain in filling factor η_R projected for this structure. The η_R was varied within the achievable range by the various RF histology coils constructed. The resulting plot was inferred using Eq. [1] and the assumption that the *Q* factor effect remained unchanged.

In comparison, the experimental measurement of the Bruker head coil demonstrated ~10% better performance (open circle) than expected due to its slightly smaller size. When examining the largest histology coil (*W* = 52 mm, IL = 24 mm, *H* = 1350 μm), a structure that can accommodate a glass histology slide with the widest RF coverage, the resulting sensitivity measured experimentally (SNR_R ~ 117%, open triangle) underperformed by nearly twofold relative to the performance expected by the quadrature coil (SNR_R ~ 238%,

black line). This sensitivity loss amounts to ~1.4 fold than what was expected (SNR_R ~170%, grey line) when accounting the linear nature of the histology resonator based on a corresponding ~5.63 × η_R improvement. Similarly, the rest of the histology coils underperformed in a comparable fashion by a factor of 1.77 in sensitivity (closed triangle) relative to the projected gain in filling factor for the quadrature coil (black curve) and by 1.26 fold when correcting for the linear detection outlined by the grey curve. The dashed line projects the theoretical sensitivity that would be gained by the largest histology coil (open triangle) when varying the gain in filling factor within the same range. Since this theoretical curve takes into account the electric loss inherent to the largest histology coil, the resulting improved performance measured with smaller structures reflects the expected decrease in losses as the coil size is reduced. This improvement is reinforced by the observed improvement of the *Q* factor measurements summarized in Figure 3 as the coil size is decreased.

These *Q* measurements were also accounted for in Figure 4 using Eq. [1] by combining the contributions from both the sensitivity inferred from the η_R (dashed line) and the corresponding Q_R measured for each coil and outlined in Figure 3. The Q_R-corrected sensitivity (open squares) demonstrated a close match with the measured experimental values for each histology coil (open and filled triangles).

To assess the role of the spacer and its effect on the performance of the coils, the layered Teflon insert (measured dielectric constant $\varepsilon \approx 1.78$) was replaced with a three-coverglass-stacked insulator (measured $\varepsilon \approx 2.69$) for the medium histology coil (*W* = 26 mm, IL = 24 mm, OL = 48 mm). This latter coil is similar in size to the one initially designed by Meadowcroft et al. (35) and dedicated to samples encased between two coverslips. This substitution resulted in a 26% relative loss in the measured sensitivity—decreasing from 321% for the Teflon spacer (Fig. 4, filled triangle) to 238% for the glass spacer (filled diamond). This substantial loss cannot be explained solely by the alteration of their quality factor ratio $Q_{L(\text{Glass spacer})}/Q_{L(\text{Teflon spacer})}$. Using Eq. [1], this Q_R decrease would have led to a marginal 3% reduction in sensitivity relative to the Teflon-based structure (Fig. 4, star), leaving a 23% loss unaccounted for. In contrast, the replacement of the spacer with an air gap interface unexpectedly resulted in a similar performance to the Teflon-based spacer (data not shown).

Examples of MRI data acquired with our various RF histology coils and thin mouse and human tissue sections that perfectly matched with their corresponding light microscopic images are shown in Figures 5–7. The sensitivity of the medium size histology coil (*W* = 26 mm, IL = 24 mm, OL = 48 mm, *H* = 450 μm) was exemplified by the acquisition of images with 50-μm in-plane resolution from 60-μm-thick tissue sections of freshly excised mouse brain and kidney using a less than 6-h imaging time (Fig. 5). The smallest and most sensitive dual-coverslip histology coil (*W* = 12 mm, IL = 12 mm, OL = 24 mm, *H* = 450 μm) can accommodate tissue portions or small organs to give the highest anatomical detail as illustrated in Figure 6. The examples shown in (a) and (b) correspond to T2*-weighted and T1-weighted images from a excised 60 μm mouse olfactory bulb mounted on dual coverslips, respectively. These results convincingly matched with their corresponding light microscopic images (c). Highly detailed coronal mouse brain sections (50-μm in-plane

resolution) were also observed using a 60-μm-thick section acquired in less than 12 h as shown in (d) T2*- and (e) T1-weighted scans. This also was in perfect alignment with (f) light microscopic imaging.

The largest coils designed in this study (W = 52 mm, IL = 24 mm, OL = 48 mm) could be used for high throughput acquisitions by scanning multiple sections at once (a–f) or to image large sized tissue (g, h). When imaging conventional premounted tissues on glass slides, sections occupying a large area (up to 30-mm wide), required an opening nearly three times the size (H = 1350 μm) as that needed for the dual-coverslip setup (H = 450 μm). This widening translated into a threefold reduction in the filling factor (η) resulting in 57% effective coil sensitivity depicted by the comparison of both coils using the same sample (Fig. 7a, b).

DISCUSSION

Despite the simplicity of our in-house slide coil design, its construction required extra precautions due to the close proximity of the sample to the surface of the copper strip. Specifically, the presence of defects within the conducting tape were visible in the MRI as field distortions or signal voids. Our successful designs, reflected by the excellent RF homogeneity shown in Figure 2, were achieved by preventing the formation of air bubble traps or the presence of unwanted impurities. The incorporation of an interchangeable T/M circuit was easy to use and exceptionally cost-effective, yet consistently resulted in very reproducible performance.

The sample preparation was crucial to obtain artifact-free MRI. Both tissue rehydration and degassing were key, especially for previously mounted samples subjected to unknown conditions. In contrast, freshly excised tissue provided the opportunity to better control the sample preparation and to achieve the greatest MRI sensitivity and the best η conditions when two coverslips were used for the setup. Importantly, the dual-coverslip design demonstrated a 1.7 fold gain in sensitivity under equal coil dimensions at the cost of a narrower opening preventing the insertion of glass slides as outlined in Figure 2 and illustrated by the examples in Figure 7a, b.

The largest planar-shaped structure constructed (W = 52 mm, IL = 24 mm) showed an unprecedented homogeneous RF geometric ratio combining a thin RF layer confined within a 450-μm opening while laterally spreading over a very large width—up to ~115 times greater than its thickness. This translated into a planar RF coverage of nearly twice the size of the largest dimensions of our mouse head reference coil (ID = 28 mm, L = 29 mm) yet providing comparable sensitivity. The relatively small size of all the samples examined led to negligible loading effects reflected by the unaffected Q factors for all of the probes but the smallest histology coil in Figure 3. The loading effect measurable in the smallest histology antenna (W = 12 mm, IL = 12 mm) can be explained by the sample volume becoming nonnegligible relative to the size of the RF resonator. This allowed for a significant gain in η_R (higher than 4-fold) relative to the nearest coil size design (medium coil: W = 26 mm, IL = 24 mm). Despite being only linear in polarization, the considerable η_R increase (higher than 132-fold factor) achieved by the histology probe resulted in an

exceptional 6.7 times gain in sensitivity relative to the whole mouse CP reference head coil. This would translate into a 9.4 times gain in sensitivity compared to a linear birdcage mouse head coil. In comparison, the study performed by Nabuurs and coworkers (36) at 400 MHz reported a 3.8-fold gain in sensitivity when inserting a self-resonant squared loop (15 × 15 mm^2) inductively coupled within a linear mouse head coil (accessible ID = 25-mm, *L* not reported) that we assume is approximately similar in size to our reference coil. Our smallest histology probe exceeded the sensitivity of a commercially available mouse head two-channel-phased surface array coil by a 3.3-fold.

The RF sensitivity factor S_{RF}, which combines both η and *Q* (28,29) proved to be reliably predictive of the SNR when accounting for the changes in coil dimensions among the histology coils designed for this study. This was illustrated in Figure 4 by the negligible deviations between the effective sensitivity of each coil measured experimentally (triangle plots) and the Q_R-corrected performance inferred from the gain in η (square plots). It must be noted that this was only observed when these structures were identical both in design and components.

In contrast, the same S_{RF} equation failed to predict the difference in performance between the commercial volume coils and the histology coils, even when accounting for quadrature vs. linear polarization by dividing the commercial coil results and extrapolations by 1.4 fold. Based on the projected gain in η_R, a systematic difference in performance (up to 1.4-fold) was observed between the sensitivity inferred from the mouse head birdcage (Fig. 4, grey line plot) and the one effectively measured in each homemade coil (Fig. 4, triangle plot). Importantly, this difference only marginally translated into changes in their corresponding *Q* factors and may partly reflect the deviation of the current via the spacer inherent to this capacitor-like structure. This was further investigated by replacing the Teflon spacer with a glass substrate for the same histology probe. Despite the 26% experimental SNR loss observed by this substitution (difference between triangle and diamond in Fig. 4), only a 3% deviation was predicted by the measured change of the Q_{Glass} factor. Notably, a residual 23% deviation remained unaccounted for by the S_{RF} equation. The relatively low performance of the glass-filled coil might be attributed to larger current deviated through the glass substrate resulting in less current flowing around the imaging compartment. Unlike in the sample compartment where the electrical properties are imposed by the nature of the tissue and the encasing, we investigated the possible improvement that may be achieved within the spacer compartment. Ideally, the layered Teflon spacer (dielectric constant measured $\varepsilon \approx 1.78$) could be replaced by a vacuum-based insert ($\varepsilon = 1$) as a potential solution to substantially reduce the spacer-driven current deviation. Instead, this was practically implemented by incorporating an air-gap spacer that we predicted would mimic the dielectric properties of vacuum ($\varepsilon \approx 1$). Our results were comparable with the performance of the Teflon spacer (data not shown). The unexpected under-performance of our homemade air-gap spacer can likely be attributed to the permittivity dependence of air to relative humidity and temperature from the surrounding atmosphere (43). Unless we can better control the media content within the gap by creating sealed air cavities, the probe will be sensitive to ambient conditions. These findings exhibit the practical utility of the Teflon spacer initially suggested by Meadowcroft et al. (35) as a robust insulator. In this type of

configuration where a spacer is required to obtain a wide RF homogeneity, Teflon will help reduce electric losses and be more resistant to atmospheric and experimental conditions.

In conclusion, our results demonstrate that the flat coils designed for this study are unique structures for the direct imaging of histology slides by offering an unrivaled trade-offs between an excellent homogenous RF coverage and an optimal filling factor. The resulting geometric efficiency was important enough to prevail over the relatively reduced electrical performance inherent to the design. The considerable gain in sensitivity (up to 6.7-fold) obtained relative to any conventional CP coil allowed for the acquisition of highly resolved images using tissue section thicknesses commonly used for histology within their standard mounting. This provided the unique opportunity to obtain unparalleled image coregistration between MRI and light microscopy that would be otherwise unachievable using conventional resonators. Our results highlight the role of the Teflon spacer as a stable insulator. Its insertion between the input port and the imaging region permitted the continuous and even distribution of the currents to ensure a homogenous RF coverage of the sample. Our findings also helped assess the extent of the losses associated with the coil's electrical inefficiency that were unaccounted for by the equation modeling the RF sensitivity.

Supplementary Material

Refer to Web version on PubMed Central for supplementary material.

Acknowledgments

Grant sponsor: Alzheimer's Association; Grant number: IIRG-08-91618; Grant sponsor: American Health Assistance Foundation; Grant number: A2008-155; Grant sponsor: NYU Applied Research Support Fund; Grant sponsor: National Cancer Institute; Grant number: 5P30CA016087-32.

The authors thank Dr. Chris Collins for his helpful discussions, feedback, and critical proofreading of this manuscript. Dr. Jose Raya is acknowledged for providing the human cartilage specimen illustrated in one of our example. The authors also extend their sincere thanks to Drs. Daniel H. Turnbull, Thomas Wisniewski, and Einar M. Sigurdsson, as well as to their respective laboratory teams, for the generous access to their laboratory and their continued help and support.

References

1. Choe AS, Gao Y, Li X, Compton BK, Stepniewska I, Anderson WA. Accuracy of image registration between MRI and light microscopy in the ex-vivo brain. Magn Reson Imag. 2011; 29:683–692.
2. Chakravarty MM, Bertrand G, Hodge CP, Sadikot AF, Collins DL. The creation of a brain atlas for image guided neurosurgery using serial histological data. NeuroImage. 2006; 30:359–376. [PubMed: 16406816]
3. Chang C, Jang T. Magnetic resonance microscopy of hamster olfactory bulb: a histological correlation. Anatom Record. 1995; 242:132–135.
4. Li X, Yankeelov TE, Rosen GD, Gore JC, Dawant BM. Enhancement of histological volumes through averaging and their use for the analysis of magnetic resonance images. Magn Reson Imag. 2009; 27:401–416.
5. Schormann T, Dabringhaus A, Zilles K. Statistics of deformations in histology and application to improved alignment with MRI. IEEE Trans Med Imag. 1995; 14:25–35.
6. Benveniste H, Kim K, Zhang L, Johnson GA. Magnetic resonance microscopy of the C57BL mouse brain. NeuroImage. 2000; 11(6 Pt 1):601–611. [PubMed: 10860789]

7. Johnson GA, Cofer GP, Fubara B, Gewalt SL, Hedlund LW, Maronpot RR. Magnetic resonance histology for morphologic phenotyping. J Magn Reson Imag. 2002; 16:423–429.
8. Johnson GA, Thompson MB, Drayer BP. Three-dimensional MRI microscopy of the normal rat brain. Magn Reson Med. 1987; 4:351–365. [PubMed: 3586982]
9. Johnson GA, Thompson MB, Gewalt SL, Hayes CE. Nuclear magnetic resonance imaging at microscopic resolution. J Magn Reson. 1986; 68:129–137.
10. Ma Y, Hof PR, Grant SC, Blackband SJ, Bennett R, Slatest L, McGuigan MD, Benveniste H. A three-dimensional digital atlas database of the adult C57BL/6J mouse brain by magnetic resonance microscopy. Neuroscience. 2005; 135:1203–1215. [PubMed: 16165303]
11. Ma Y, Smith D, Hof PR, Foerster B, Hamilton S, Blackband SJ, Yu M, Benveniste H. In vivo 3D digital atlas database of the adult C57BL/6J mouse brain by magnetic resonance microscopy. Front Neuroanat. 2008; 2:1–10. [PubMed: 18958199]
12. Wu N, Peck TL, Webb AG, Magin RL, Sweedler JV. 1H-NMR Spectroscopy on the nanoliter scale for static and online measurements. Anal Chem. 1994; 66:3849–3857.
13. Wu N, Peck TL, Webb AG, Magin RL, Sweedler JV. Nanoliter volume sample cells for 1H NMR: Application to online detection in capillary electrophoresis. J Am Chem Soc. 1994; 116:7929–7930.
14. Olson DL, Lacey ME, Sweedler JV. High-resolution microcoil NMR for analysis of mass-limited, nanoliter samples. Anal Chem. 1998; 70:645–650. [PubMed: 9470492]
15. Peck TL, Magin RL, Lauterbur PC. Design and analysis of microcoils for NMR microscopy. J Magn Reson B. 1995; 108:114–124. [PubMed: 7648010]
16. Webb AG, Grant SC. Signal-to-noise and magnetic susceptibility trade-offs in solenoidal microcoils for NMR. J Magn Reson B. 1996; 113:83–87. [PubMed: 8888593]
17. Stocker JE, Peck TL, Webb AG, Feng M, Magin RL. Nanoliter volume, high-resolution NMR microspectroscopy using a 60-micron planar microcoil. IEEE Trans Biomed Eng. 1997; 44:1122–1127. [PubMed: 9353992]
18. Lacey ME, Subramanian R, Olson DL, Webb AG, Sweedler JV. High-resolution NMR spectroscopy of sample volumes from 1 nL to 10 μL. Chem Rev. 1999; 99:3133–3152. [PubMed: 11749512]
19. Demas V, Bernhardt A, Malba V, Adams KL, Evans L, Harvey C, Maxwell RS, Herberg JL. Electronic characterization of lithographically patterned microcoils for high sensitivity NMR detection. J Magn Reson. 2009; 200:56–63. [PubMed: 19581116]
20. Webb AG. Radiofrequency microcoils for magnetic resonance imaging and spectroscopy. J Magn Reson. 2013; 229:55–66. [PubMed: 23142002]
21. Dauguet J, Delzescaux T, Conde F, Mangin JF, Ayache N, Hantraye P, Frouin V. Three-dimensional reconstruction of stained histological slices and 3D non-linear registration with in-vivo MRI for whole baboon brain. J Neurosci Methods. 2007; 164:191–204. [PubMed: 17560659]
22. Lebenberg J, Herard AS, Dubois A, Dauguet J, Frouin V, Dhenain M, Hantraye P, Delzescaux T. Validation of MRI-based 3D digital atlas registration with histological and autoradiographic volumes: an anatomofunctional transgenic mouse brain imaging study. NeuroImage. 2010; 51:1037–1046. [PubMed: 20226256]
23. Prima S, Ourselin S, Ayache N. Computation of the mid-sagittal plane in 3-D brain images. IEEE Trans Med Imag. 2002; 21:122–138.
24. Yelnik J, Bardinet E, Dormont D, Malandain G, Ourselin S, Tande D, Karachi C, Ayache N, Cornu P, Agid Y. A three-dimensional, histological and deformable atlas of the human basal ganglia. I. Atlas construction based on immunohistochemical and MRI data. NeuroImage. 2007; 34:618–638. [PubMed: 17110133]
25. Bock NA, Kovacevic N, Lipina TV, Roder JC, Ackerman SL, Henkelman RM. In vivo magnetic resonance imaging and semiautomated image analysis extend the brain phenotype for cdf/cdf mice. J Neurosci. 2006; 26:4455–4459. [PubMed: 16641223]
26. Henkelman RM. Systems biology through mouse imaging centers: experience and new directions. Ann Rev Biomed Eng. 2010; 12:143–166. [PubMed: 20415591]
27. Durgun-Yucel B, Hopwood D, Yucel AH. The effects of mercaptoethanol-formaldehyde on tissue fixation and protein retention. Histochem J. 1996; 28:375–383. [PubMed: 8818684]

28. Tsunoda S, Martin CJ. Lung tissue shrinkage after freeze substitution for histologic study. Am Rev Respir Dis. 1973; 107:876–878. [PubMed: 4572024]
29. Lum H, Mitzner W. Effects of 10% formalin fixation on fixed lung volume and lung tissue shrinkage. A comparison of eleven laboratory species. Am Rev Respir Dis. 1985; 132:1078–1083. [PubMed: 4062038]
30. Jonmarker S, Valdman A, Lindberg A, Hellstrom M, Egevad L. Tissue shrinkage after fixation with formalin injection of prostatectomy specimens. Virchows Archiv. 2006; 449:297–301. [PubMed: 16909262]
31. Blasdale C, Charlton FG, Weatherhead SC, Ormond P, Lawrence CM. Effect of tissue shrinkage on histological tumour-free margin after excision of basal cell carcinoma. Br J Dermatol. 2010; 162:607–610. [PubMed: 19906070]
32. Cutts A. Shrinkage of muscle fibres during the fixation of cadaveric tissue. J Anatomy. 1988; 160:75–78.
33. Fukaya H, Martin CJ. Lung tissue shrinkage for histologic preparations. Am Rev Respir Dis. 1969; 99:946–948. [PubMed: 4892104]
34. Meadowcroft MD, Connor JR, Smith MB, Yang QX. MRI and histological analysis of beta-amyloid plaques in both human Alzheimer's disease and APP/PS1 transgenic mice. J Magn Reson Imag JMRI. 2009; 29:997–1007.
35. Meadowcroft MD, Zhang S, Liu W, Park BS, Connor JR, Collins CM, Smith MB, Yang QX. Direct magnetic resonance imaging of histological tissue samples at 3. 0T. Magn Reson Med. 2007; 57:835–841. [PubMed: 17457873]
36. Ippel JH, Koutsopoulos S, Nabuurs SM, van Berkel WJ, van der Oost J, van Mierlo CP. NMR characterization of a 264-residue hyperther-mostable endo-beta-1,3-glucanase. Biochem Biophys Res Commun. 2010; 391:370–375. [PubMed: 19913513]
37. Styles P, Scott CA, Radda GK. A method for localizing high-resolution NMR spectra from human subjects. Magn Reson Med. 1985; 2:402–409. [PubMed: 4094554]
38. Darrasse L, Ginefri JC. Perspectives with cryogenic RF probes in biomedical MRI. Biochimie. 2003; 85:915–937. [PubMed: 14652180]
39. Hoult DI, Richard RE. The signal-to-noise ratio of the nuclear magnetic resonant experiment. J Magn Reson. 1983; 24:71–85.
40. Mispelter, J.; Lupu, M.; Briguet, A. NMR Probeheads for biophysical and biomedical experiments. London: Imperial College Press; 2006.
41. Wadghiri YZ, Hoang DM, Wisniewski T, Sigurdsson EM. In vivo magnetic resonance imaging of amyloid-beta plaques in mice. Methods Mol Biol. 2012; 849:435–451. [PubMed: 22528108]
42. Ernst RR, Anderson WA. Application of Fourier transform spectroscopy to magnetic resonance. Rev Sci Instrum. 1966; 37:93–102.
43. Zarnik MS, Belavic D. An experimental and numerical study of the humidity effect on the stability of a capacitive ceramic pressure sensor. Radioengineering. 2012; 21:201–206.

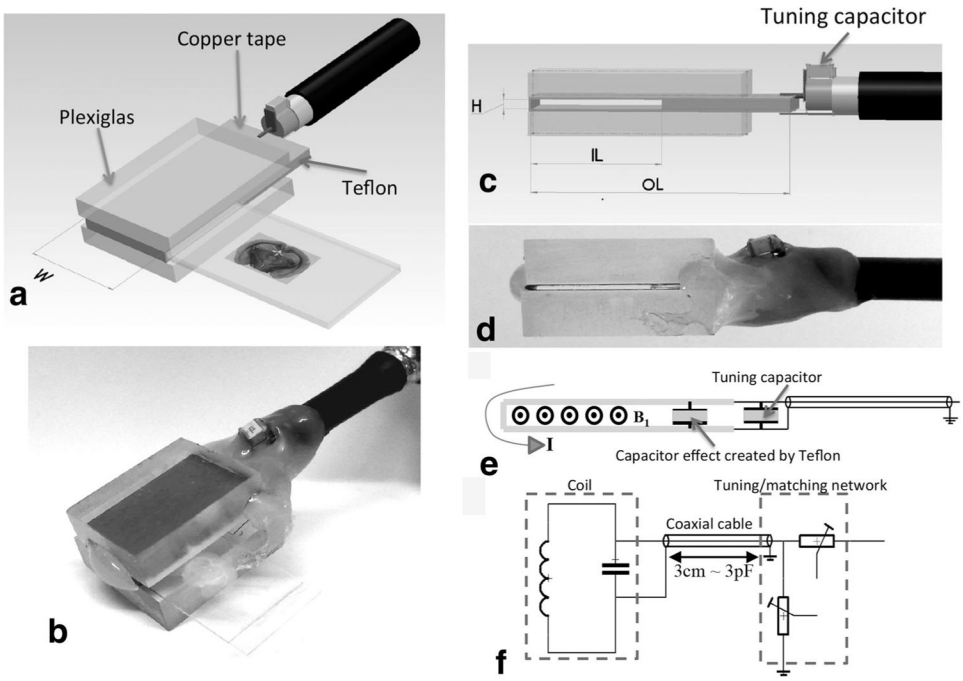

FIG. 1.

Principle and overview of the histology slide probe. **a**: Schematic of the planar coil structure to accommodate histology tissue section. The choice of the width (*W*) defines the extent of the homogeneous RF field of interest covering the tissue sample to be imaged within a slide. **b**: The height (*H*) of the opening was chosen to insert a tissue encasing slide setup to accommodate the pairing of either a glass/coverslip (~1350 μm) or two coverslips (~450 μm). **c**: The inner length (IL) comes in two dimensions to house commercially available 12-mm-wide coverslips or 25-mm-wide slides. The resulting OL of the probe is approximately twice the IL as prescribed by Meadowcroft et al. (2007). For the sake of simplicity of the design, the construction of the structures described in this work was made in-house using thermo-glue as in (b and **d**). **e**: The current traversing the slotted resonator induces a transverse B1 RF field after crossing a square Teflon-based capacitive insert extending throughout the whole unused but required OL of the coil. **f**: The tuning/matching (T/M) of all the probes is insured by two variable capacitors (Voltronics Corps., Salisbury, MD) via a double-shielded coaxial cable. All probes can be easily interchanged with the same T/M circuit.

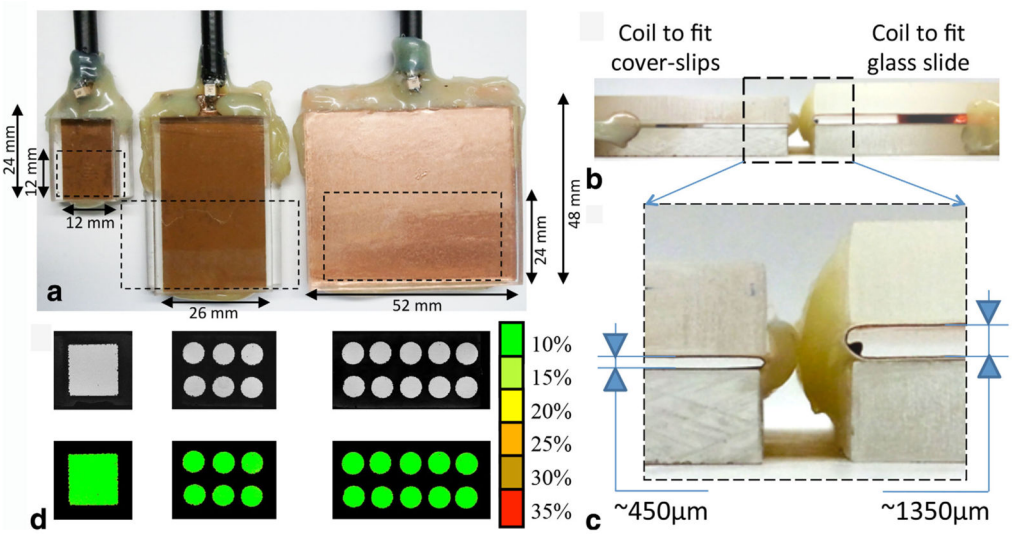

FIG. 2.

A set of five histological slide coils were developed to accommodate both different sample sizes and slide setup. **a**: The coils were designed in three sizes to house encasing based on dual coverslips for tissue sections up to 100 µm thick (insert $H \approx 450$ µm). The smallest coil (left: W = IL = 12 mm, OL = 24 mm) was designed to insert 24 × 12 mm coverslips. The middle coil shown is of similar size (W = 26 mm, IL = 24 mm, OL = 48 mm) to the structure previously reported (35) to enable the partial examination of standard size slides (50 × 24 mm). The larger structure (W = 52 mm, IL = 24 mm, OL = 48 mm) shown at right permits the full coverage of slides of the same size. **b**: Another two coils with identical size to the two largest probes were additionally designed with a greater height ($H \approx 1350$ µm instead of $H \approx 450$ µm) to fit the coverslip/glass slide set up. **c**: All the coils proved to have an excellent RF planar homogeneity assessed experimentally using MRI with a phantom composed by a thin layer of water doped with 2.5 mM Gd-DTPA sandwiched between two coverslips. As indicated in the color scale, the green level represents less than 10% deviation from the average signal intensity measured by the ROI outlined in the map (white dashed line).

RF MRI Probe	η_R (Relative to commercial mouse head coil)	Q_u (Unloaded - Air)	Q_L (Loaded with Mouse Brain tissue section)	Q_R (Relative to commercial mouse head coil)	Sensitivity (S_R) (Measured SNR ratio relative to commercial mouse head coil)
Doty Mouse whole Head Probe (Doty Scientific Inc.) ID=28-mm, L=29-mm	1.0	145.0	145.0	100%	100%
Bruker Mouse whole Head Probe (Bruker Biospin) Bircage CP coil ID=24.5-mm, L=28-mm, Model No. 1P T20063V3	1.3	*	*	*	111%
Bruker Mouse Head Surface Probe (Bruker Biospin) 2-ch phased array Coil (Model No. 1P T11204V3) W_x=27-mm, L_z=19-mm,curvature ID=25-mm.	**	*	*	*	226%
Large Glass Slide coil Insert: W=52-mm, IL=24-mm,H=1,350µm. Overall Length: W=52-mm, OL=48-mm.	5.6	83.0	83.0	57%	117%
Medium Glass Slide coil Insert: W=26-mm, IL=24-mm,H=1,350µm. Overall Length: W=26-mm, OL=48-mm.	12.2	102.0	102.0	70%	199%
Large coverslip coil Insert: W=52-mm, IL=24-mm,H=450µm. Overall Length: W=52-mm, OL=48-mm.	14.7	86.0	86.0	59%	208%
Medium coverslip coil Insert: W=26-mm, IL=24-mm,H=450µm. Overall Length: W=26-mm, OL=48-mm.	31.8	104.0	104.0	72%	321%
Medium coverslip coil (Glass spacer) Insert: W=26-mm, IL=24-mm,H=450µm. Overall Length: W=26-mm, OL=48-mm.	31.8	98.0	98.0	68%	238%
Medium coverslip coil (Air gap spacer) Insert: W=26-mm, IL=24-mm,H=450µm. Overall Length: W=26-mm, OL=48-mm.	31.8	106.0	106.0	73%	308%
Small coverslip coil Insert: W=12-mm, IL=12-mm,H=450µm. Overall Length: W=12-mm, OL=24-mm.	132.3	115.0	112.0	77%	670%

FIG. 3.

Summary of the main physical coil dimensions, the geometrical sample matching via the relative filling factor η_R as well as the RF characteristics (Q_U, Q_L, and Q_R) of all the coils considered in this study. The measurement of the Q factor of each coil was assessed systematically several times both unloaded and loaded showing negligible variations (less than 0.5%). No loading effect was noticeable when inserting the sample in any of the resonator but in the smallest coil (3% between unloaded and loaded). The measured sensitivity of each resonator is reported relative to a commercial coil (here a mouse head coil from Doty Scientific, Inc.) used as a reference. Some of the characteristics for the commercial Bruker coils are not reported due to our inability to measure the corresponding parameters under the same conditions due to the electrical circuit setup (*) or to the open nature of the surface structure generating an inhomogeneous RF field (**).

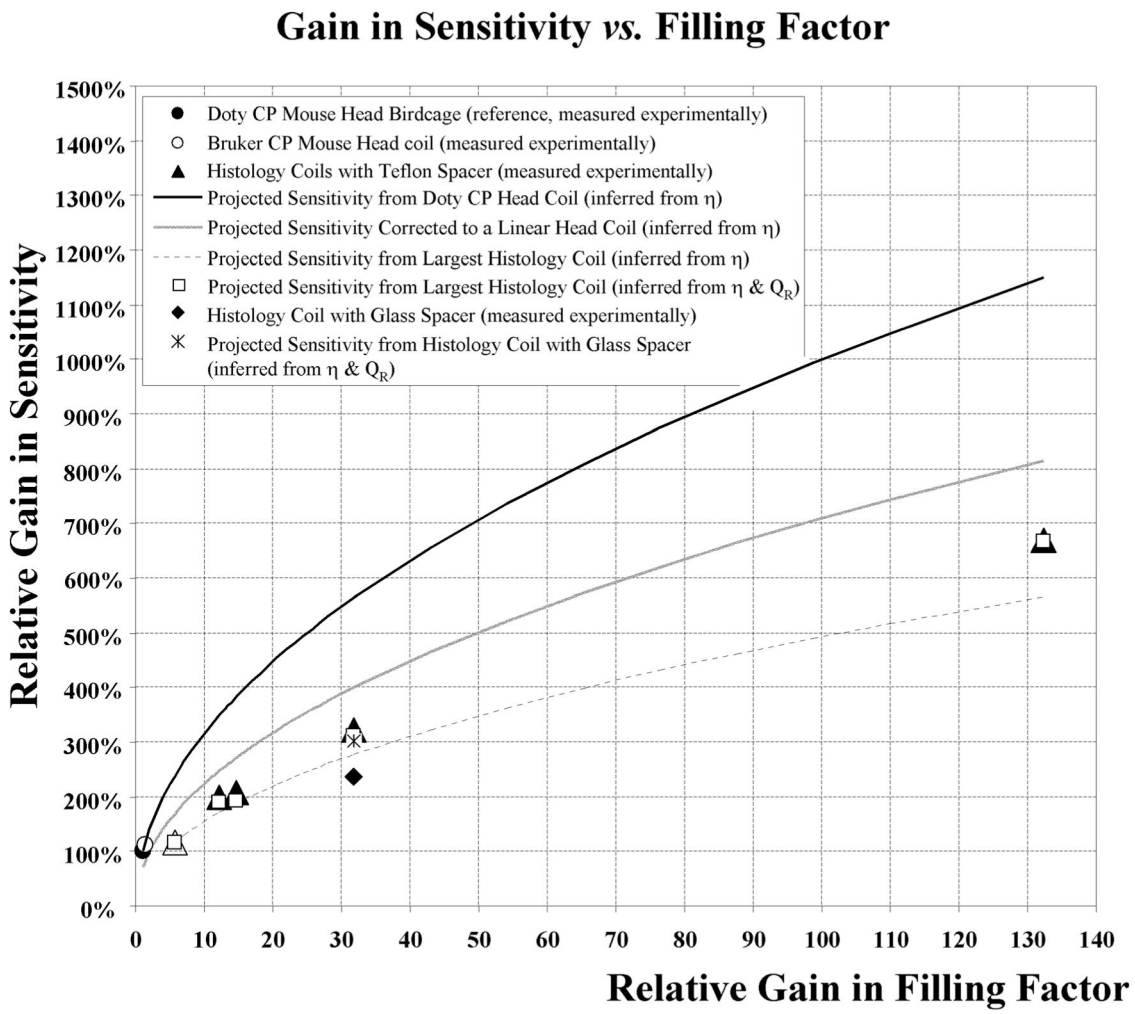

FIG. 4.

Summary of the sensitivity of all the coils utilized in this study (Commercial Birdcage coils: open and filled circles, Histology coils: open and filled triangles and diamond) as a ratio of the effective SNR to that of a commercial mouse head RF coil used as our reference (filled circle) using the same sample for all coils. The solid black line depicts the projected increase in sensitivity of the reference CP birdcage coil that would result from the gain in filling factor achievable by the various RF histology coil using equation [1] (here *Q* is unaccounted for). The grey line is the sensitivity scaled down by 1.4 in the case of a linear birdcage coil structure. The difference between the grey line and triangles illustrates the systematic underperformance of the histology coils by a factor up to 1.4-fold compared with the linear birdcage coil structure. Similarly, the dashed line plot was inferred using the measured sensitivity of the largest histology coil (open triangle) as the baseline. All lines were calculated with the assumption that the effect of the *Q* factor remained unchanged. The dashed line curve also showed a deviation from the measured values (triangles) but this time the flat histology coil structures exhibited improved performance as the measured *Q* increased as their size decreased. Using Eq. [1], this difference was accounted for by incorporating the relative experimentally measured Q_R, resulting in values (open squares) in good agreement with measured SNR (open and filled triangles). The substitution of the Teflon spacer by a three-layer glass insert while maintaining the identical filling factor resulted in a 26% measured loss of relative sensitivity (filled diamond). However, the corresponding *Q* factor relative to the Teflon spacer exhibited only a 6% decrease that should lead to only a 3% drop (star) according to Eq. [1] leaving 23% loss unaccounted for. In contrast, the replacement of the Teflon with an air gap insert led to a negligible change (data not shown).

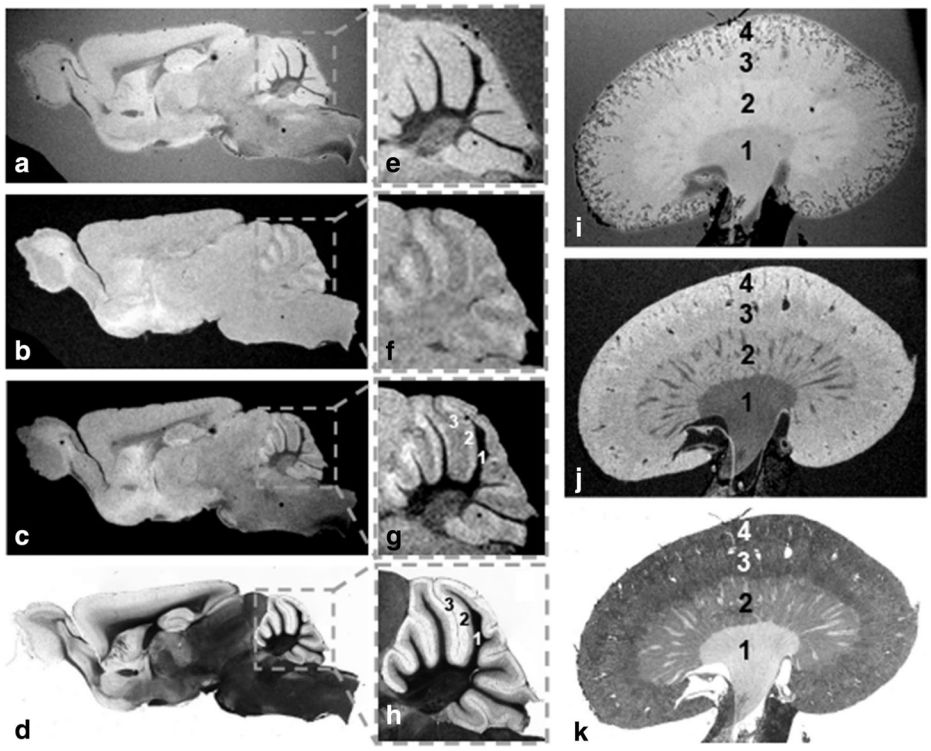

FIG. 5.

Examples of T2*-weighted (**a**) and T1 weighted (**b**) images from 60 μm mid-sagittal section of a whole brain obtained from a wild-type mouse were acquired with the medium size histology coil (*W* = 26 mm, IL = 24 mm, OL = 48 mm, *H* = 450 μm). Each image contrast was acquired with a 50 μm in-plane resolution image in less than 6 h (totaling 12 h). The overlaying of both MRI contrast (**c**) help identify some of the anatomical details seen with the near perfectly matched light microscopy (**d**). This can be better appreciated with the boxed view at the cerebellar level (**e–h**) in which the various cell layers (1: cerebellar white matter, 2: molecular cell layer, and 3: granular cell layer) are better seen when combining T2*- and T1-weighting contrast. The same procedure was repeated for a 60-μm mouse kidney sample using both a T2*-weighted (**i**) and a T1-weighted (**j**) contrast where the main anatomical areas of this organ can be identified (1: pelvis, 2: medulla, 3: cortex, and 4: capsule) and perfectly co-registered with histology (**k**).

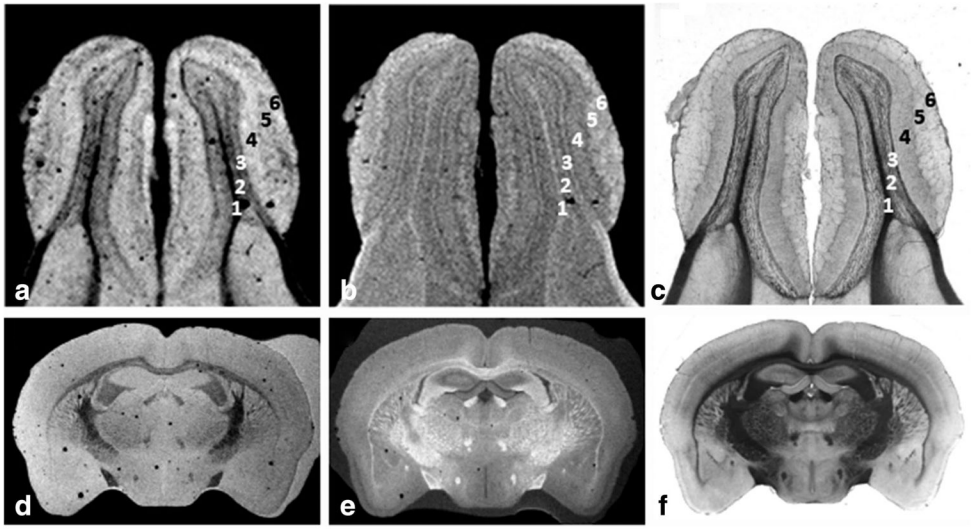

FIG. 6.

The highly detailed image examples shown were obtained from 60 μm tissue sections using the smallest and most sensitive coverslip histology coil designed in this study (W = 12 mm, IL = 12 mm, OL = 24 mm, H = 450 μm). The first image set (**a**) and (**b**) correspond respectively to T2*- and T1-weighted images with 30 μm in-plane resolution obtained from the mouse olfactory bulb coregistered with the corresponding light microscopy (**c**). The MRI contrast on both images helps identify the following cell layers: (1) olfactory ventricle, (2) combines the internal plexiform layer, granule cell layer and ependymal layer, (3) mitral cell layer, (4) external plexiform layer, (5) glomerular layer, (6) olfactory nerve layer. The coil can also accommodate coronal mouse brain sections depicted by the example of a 50-μm in-plane MRI showing clearly the white matter track and different small tissue structures in (**d**) T2*- and (**e**) T1-weighted images in perfect alignment with (**f**) histology.

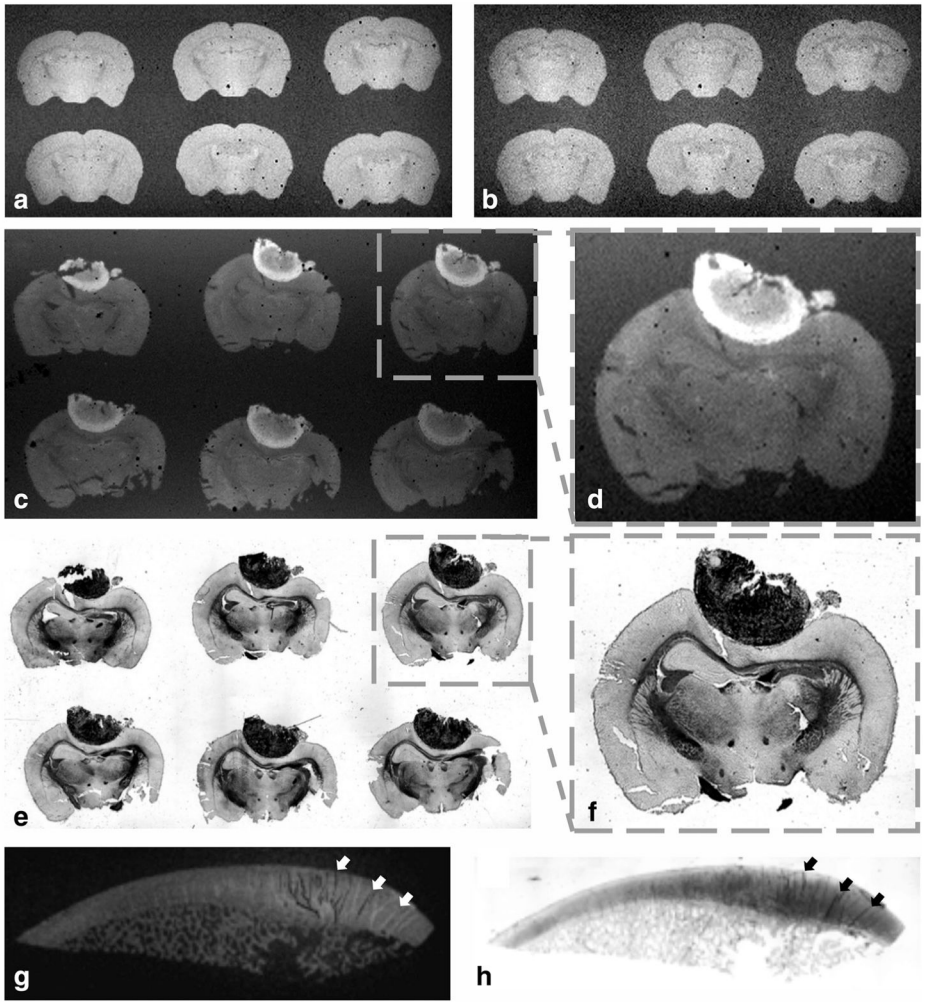

FIG. 7.

Both large coverslip and glass-slide coils can be used for high throughput acquisitions by scanning simultaneously multiple tissue sections (**a–f**). This setup can also accommodate large size samples (**g–h**). The difference in SNR between T2*-weighted brain images acquired in (a) SNR = 47 and (b) SNR = 28 illustrates the 3× greater filling factor of the dual coverslip coil (W = 52 mm, IL = 24 mm, OL = 48 mm, H = 450 μm) compared with the identical structure but capable of housing samples embedded in traditional coverslip/glass slide setup that are much thicker (coil with equal dimensions but H = 1350 μm). The example shown in (c) depicts the T1 brightening of a melanoma tumor in a set of 6 × 40 μm mouse brain sections premounted in a glass slide and acquired with a 60-μm in-plane resolution where (d) corresponds to a magnification of the boxed area in (c) and (e and f) the matched histology. The image example in (g) corresponds to a 100-μm in-plane gradient echo image of a 5-μm human trochlear cartilage (SNR = 33 for an 8 h scanning time) and (h) histology of the same sample using Alcian blue dye to stain glycosaminoglycans and help identify the loss of in cartilage integrity highlighted by the contrast from both imaging modality depicted by the arrows in g and h.